IEEE Access
Multidisciplinary | Rapid Review | Open Access Journal

Received July 18, 2017, accepted August 21, 2017, date of publication August 31, 2017, date of current version September 27, 2017.

Digital Object Identifier 10.1109/ACCESS.2017.2748057

Performance Analysis of Layered ACO-OFDM

XIAOYU ZHANG, (Student Member, IEEE), QI WANG, (Member, IEEE), RONG ZHANG, (Senior Member, IEEE), SHENG CHEN, (Fellow, IEEE), AND LAJOS HANZO, (Fellow, IEEE)

School of Electronics and Computer Science, University of Southampton, Southampton, SO17 1BJ, U.K.

Corresponding author: Lajos Hanzo (lh@ecs.soton.ac.uk)

This work was supported in part by the Engineering and Physical Sciences Research Council under Project EP/N004558/1 and Project EP/N023862/1, in part by the R.A.Eng. Industrial Fellowship, in part by the European Research Councils Advanced Fellow Grant through the Beam-Me-Up Project, and in part by the Royal Society Wolfson Research Merit Award. The work of L. Hanzo was supported by the European Research Councils Senior Research Fellow Grant.

ABSTRACT Layered asymmetrically clipped optical orthogonal frequency division multiplexing (LACO-OFDM) has been proposed for improving the spectral efficiency of conventional asymmetrically clipped optical OFDM. Multiple base layers that are orthogonal in the frequency domain are sequentially superimposed to form LACO-OFDM, where each superimposed layer fills the empty subcarriers left by the previous layer. As our contribution, the bit error ratio (BER) considering the effect of thermal noise, clipping distortion, inter-layer interference, and the bit rate difference between layers is analysed in this paper. Since the BER performance of LACO-OFDM is closely related to its peak-to-average power ratio (PAPR) distribution, we also provide the analytical expression of the PAPR distribution in this paper, which quantifies how the number of layers in LACO-OFDM reduces the PAPR. As a further advance, we propose a tone-injection aided PAPR reduction design for LACO-OFDM, which in turn improves the BER performance. Simulations are provided for verifying both the analytical BER performance and the PAPR distribution of LACO-OFDM. The results show that the expressions derived match well with the simulations. Furthermore, the PAPR reduction method proposed attains a 5 dB PAPR reduction at the 10^{-3} probability-point of the complementary cumulative distribution function, as well as a better BER performance than the original LACO-OFDM scheme.

INDEX TERMS Layered asymmetrically clipped optical orthogonal frequency division multiplexing (LACO-OFDM), bit error ratio (BER), inter-layer interference, clipping distortion, peak-to-average power ratio (PAPR), tone injection.

I. INTRODUCTION

In recent years, the ever-growing urban population density, the portable device usage and multimedia streaming requirements result in increased tele-traffic [1], [2]. As a remedy, the unregulated visible light band is gaining research attention as an appropriate alternative. Light-emitting diodes (LED) act as downlink transmitters in visible light communications (VLC) [2].

In VLC, intensity modulation combined with direct detection (IM/DD) has been commonly adopted to relax the complexity of the optical transceiver frontend design [3]. Since the intensity of light wave has to be non-negative, unipolar encoding is required for IM/DD transmission. In order to enhance the bandwidth efficiency, optical orthogonal frequency division multiplexing (O-OFDM) has been proposed for appropriately migrating the mature OFDM scheme from the radio frequency (RF) system to the VLC downlink, owing to its ability to mitigate the multipath-induced inter-symbol interference (ISI) [4]. Explicitly, since OFDM produces complex-valued time-domain (TD) symbols, we have to ensure that the output signal meets the unipolar IM/DD requirement.

Carruthers and Kahn [5] utilised Hermitian symmetry to generate a real-valued TD signal, which was then positively biased with a direct current (DC) component so that the signal became positive. The resultant scheme is referred to as DC-biased optical OFDM (DCO-OFDM). However, DCO-OFDM has a low energy efficiency due to its high DC energy. [6]. The more energy-efficient asymmetrically clipped optical OFDM (ACO-OFDM) was then proposed by Armstrong and Lowery [7]. In ACO-OFDM, all subcarriers having even indices are left zero, whilst addition-

ally obeying the Hermitian symmetry, as in DCO-OFDM. The corresponding TD ACO-OFDM signal is then not only real-valued, but also anti-symmetric with respect to the horizontal axis, whose negative part can be clipped at the transmitter (TX) and recovered losslessly at the receiver (RX) without additional DC shifting. Similar characteristic features are exhibited by the pulse-amplitude-modulated discrete multitone (PAM-DMT) scheme, where the imaginary part of all subcarriers is actively modulated, while the real part is left blank [8]. Diverse schemes have been advocated for avoiding the DC energy wastage, such as Flip-OFDM/U-OFDM, which transmits the positive and inverted negative parts of the real-valued symbols separately in the TD [9], [10]. Armstrong and Schmidt [6] and Armstrong *et al.* [11] carried out the bit error ratio (BER) performance analysis of DCO-OFDM and ACO-OFDM, respectively, and compared their optical efficiency to that of on-off keying. In [12] the clipping distortions in DCO- and ACO-OFDM were also taken into consideration by Dimitrov *et al.* and the clipping effects together with the BER expression of both AWGN and fading channels were also provided.

However, O-OFDM also has some impediments, such as its high peak-to-average power ratio (PAPR), which is defined as the quotient of the maximum to the average power of the TD symbols [13]. Conventional RF-OFDM systems have a high PAPR, which is further increased as the number of subcarriers increases. Hence, the TX power amplifiers have to rely on a backoff and therefore the RX analogue-to-digital converters suffer from an increased granular noise [13]. For this reason, plenty of literature can be found on the PAPR reduction of OFDM in RF systems [14]–[16]. The situation in IM/DD systems is even worse, because the lifespan of LED emitters and the overall indoor lighting functionality would be affected by the high PAPR. However, the PAPR analysis of RF OFDM signals cannot be applied to the IM/DD optical scenario due to its unipolar nature [2], [14]. A study by Wang *et al.* [17] has characterised the PAPR performance of several typical O-OFDM schemes, such as DCO-/ACO-/Flip-OFDM and PAM-DMT, where the complementary cumulative distribution function (CCDF) expressions have been derived and verified by simulations. Given the unipolar nature of the IM/DD optical signals, several methods such as null subcarrier shifting [18], pilot-symbol assistance [19] and tone injection [20] were proposed. Whilst some of the O-OFDM schemes mentioned before, such as for example ACO-OFDM, are capable of achieving a fairly high energy efficiency, the price paid is to have its spectrum efficiency halved compared to DCO-OFDM using the same constellation size [4].

Based on the aforementioned schemes, some further improved structures have also been conceived, such as asymmetrically clipped DC biased optical OFDM (ADO-OFDM) [21] and hybrid asymmetrically clipped optical orthogonal frequency division multiplexing (HACO-OFDM) [22] relying on the PAPR reduction method of [23], both of which attain a better spectral efficiency than ACO-OFDM, despite their lower energy consumption compared to DCO-OFDM. The PAPR reduction solution of Li *et al.* [23] relies on the tone-injection method originally proposed in [16] for the complex TD signals of RF-OFDM, which was then adapted. The author adjusted the method for the unipolar HACO-OFDM TD signals composed of an ACO-OFDM and a PAM-DMT base layer signal. Other approaches such as anti-periodic OFDM [24], spectral and energy efficient OFDM (SEE-OFDM) [25], enhanced U-OFDM (eU-OFDM) [26], enhanced asymmetrically clipped optical OFDM (eACO-OFDM) [27] and augmented spectral efficiency discrete multitone (ASE-DMT) [28] are also found in recent studies.

A further design option is contributed by the recently proposed layered ACO-OFDM (LACO-OFDM) [29], which populates the idle subcarriers of ACO-OFDM by creating an *additional layer* and mapping an extra set of symbols to the un-populated positions of the ACO-OFDM scheme [29], [30]. To elaborate, the LACO-OFDM distinguishes itself from other derived schemes by its flexibility, since the number of layers, the modulation scheme and power allocated to each layer can be adjusted as required, which provides more design freedom for the communication system. A study by Lowery [31] has embodied the excellent spectrum efficiency of LACO-OFDM compared with DCO-OFDM, while in [32] experiments were conducted to show the better performance of LACO-OFDM compared to DCO-OFDM. Naturally, the layered nature of the LACO-OFDM signal composition also leads to a significantly different statistical characteristics with respect to the Gaussian or truncated Gaussian distributions of the aforementioned schemes. This makes the reduction of PAPR in LACO-OFDM more difficult, since most of the methods proposed for O-OFDM only perform well for the Gaussian distribution, which is not the case for the multiple layers of LACO-OFDM and for the solution conceived in [23] for HACO-OFDM, which is composed of two base layers of equal weight.

Against this background, the BER performance of LACO-OFDM is analysed in the face of thermal noise, inter-layer interference and clipping distortion. The bit rate difference between layers is also quantified. Its BER expression is also provided, which suggests that the clipping becomes a major performance-limiting factor in the high signal-to-noise ratio (SNR) region. Since the clipping distortion is closely related to the PAPR of the signal, the probability density function (PDF) of the PAPR is studied. A novel PAPR reduction method based on tone-injection is also proposed for improving the performance of LACO-OFDM, which formulates an optimisation problem that may be solved by off-the-shelf tools, regardless of the number of layers. Monte-Carlo simulations are conducted to verify the PAPR and BER analysis.

The contributions of this paper are listed as follows.

1) The BER performance of LACO-OFDM is analysed in the face of thermal noise, inter-layer interference and clipping distortion. The bit rate difference between layers is also quantified and its BER expression is provided, which suggests that the clipping distortion

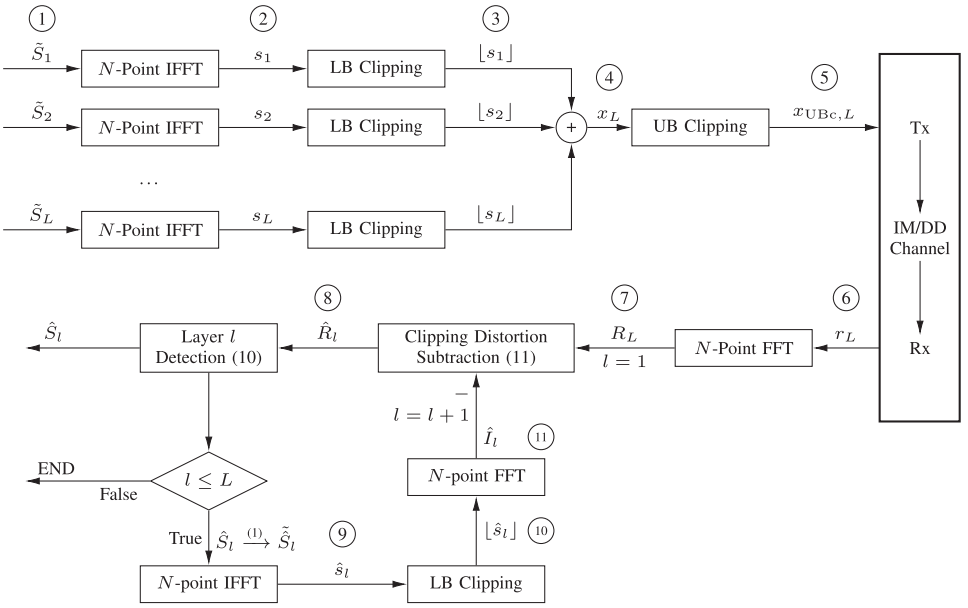

FIGURE 1. LACO-OFDM in IM/DD optical communication systems, where LB and UB clipping represent clipping at lower- and upper-boundary, respectively.

becomes a major performance-limiting factor in the high-SNR region.

2) A novel PAPR reduction method based on tone-injection is also proposed for improving the performance of LACO-OFDM, which formulates an optimisation problem that may be solved by off-the-shelf tools, regardless of the number of layers.

Monte-Carlo simulations are conducted to verify the PAPR and BER analysis.

The structure of this paper is as follows. In Section II the multi-layer LACO-OFDM is reviewed and some key points are indicated. The analysis of the LACO-OFDM BER and PAPR distribution is given in Sections III and IV, respectively. A novel PAPR reduction method is proposed in Section V for improving the system performance, while Section VI provides our simulation results for verifying the theoretical analysis. Finally, our conclusions are offered in Section VII.

II. SYSTEM MODELS

Figure 1 shows the basic schematic of a LACO-OFDM communications system, which has N OFDM subcarriers, and the final signal is composed of a total of L layers [29]. More specifically, in Fig. 2 we present side-by-side frequency and time domain views of the TX and RX processes for a LACO-OFDM signal that is composed of 3 layers and uses 16-point FFT. The remainder of this section introduces each of the steps numbered in both figures.

① At the TX side, the serially modulated frequency domain (FD) symbol stream generated from the symbol set $\mathcal{S}$ is firstly converted into parallel streams mapped to the layers. ACO-OFDM having N subcarriers is applied to the first layer, which is capable of accommodating $N/4$ symbols. This will leave $N/2$ empty subcarriers according to ACO-OFDM, which can be filled by the ACO-OFDM scheme in the second layer. In this way, the number of symbols loaded onto each of the higher layers is halved with respect to the former, i.e. the lth layer only has $N_l = N/2^{l-1}$ subcarriers for $N_l/4$ symbols. On each layer, the symbols themselves (S), together with their conjugates (S^*, shown as shaded bricks in Fig. 2 ①) generated for satisfying the Hermitian symmetry are aligned with their corresponding FD subcarriers, while the unused FD positions are left zero. For a total of $N_l/4$ multicarrier symbols on the lth layer, denoted by $S_l[k]$, $(0 \leq k \leq N_l/4 - 1)$, the length-$N$ FD signal assembled becomes:

$$\tilde{S}_l[m] = \begin{cases} S_l[k], & m = 2^l k + 2^{l-1}, \\ S_l^*[k], & m = N_l - (2^l k + 2^{l-1}), \\ 0, & \text{otherwise.} \end{cases} \quad (1)$$

② For each layer, the signal $\tilde{S}_l$ is transformed by an N-point IFFT to generate the layered TD signals s_l, where l is the index of the layer. The resultant layered signals exhibit the half-wave symmetry of ACO-OFDM, which is also shown in Fig. 2 ②. Further, the high layer signals tend to repeat themselves for several times.

③ These TD signals are then clipped at the lower boundary (LB) to zero. The resultant non-negative signals are denoted as $\lfloor s_l \rfloor$, where $\lfloor \cdot \rfloor$ stands for LB clipping. Naturally, this clipping imposes distortions on each of these signals, which appear in the FD at the specific subcarriers that were originally left blank by the current

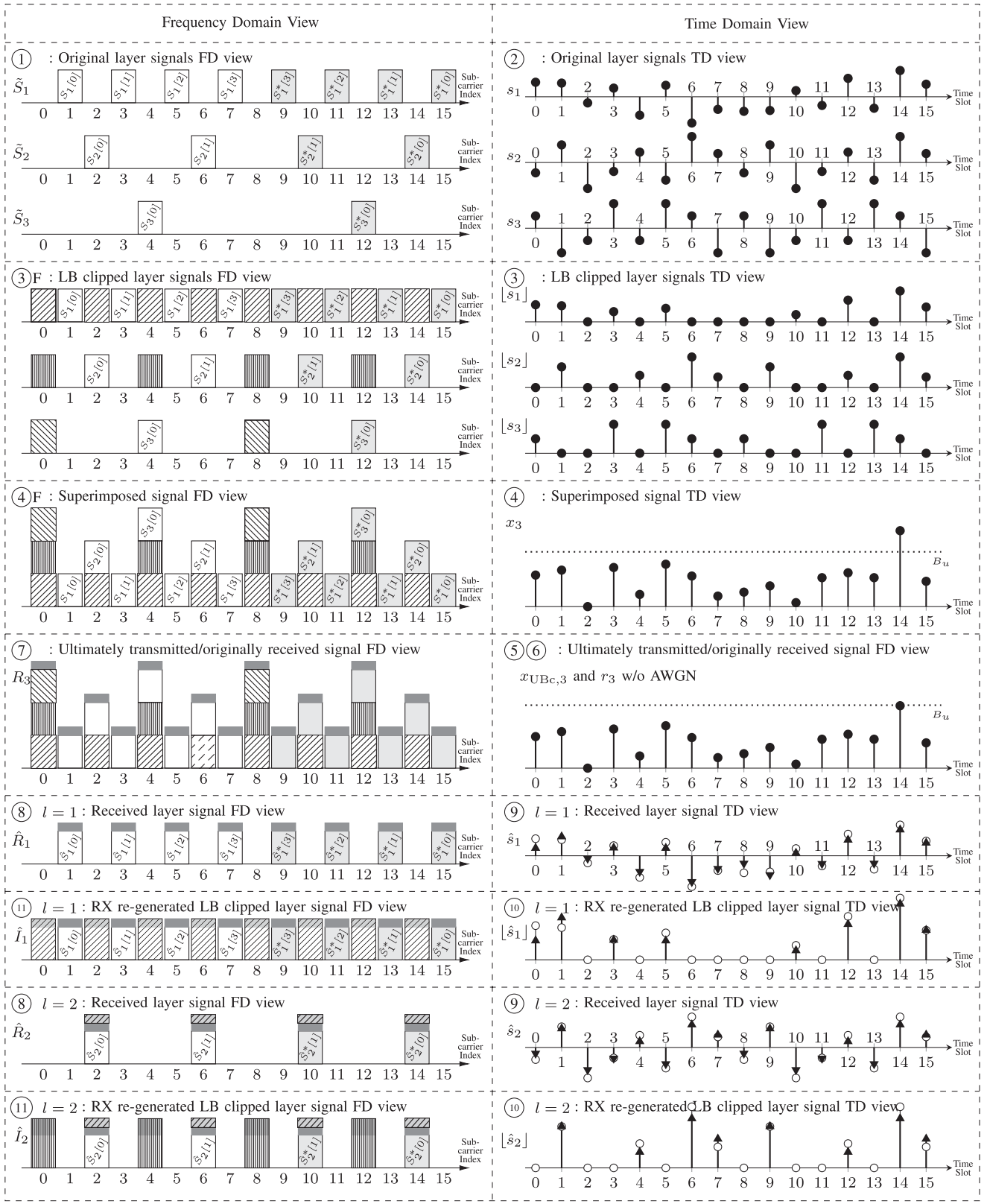

FIGURE 2. Frequency and time domain views of a 3LACO-OFDM signal with 16-point FFT. The circled numbers and the symbol notations follow those defined in Fig. 1. For the frequency domain views on the left, the purely light shaded bricks with '*' symbols are the Hermitian symmetry conjugates, while the North East hatching, vertical hatching and North West hatching represent distortion generated by Layer 1, 2 and 3, respectively. The dark grey bricks are the UB clipping distortions and the light grey bricks with lines patterns are the inheriting distortions generated by corresponding layers. For the time domain views on the right, B_u stands for the UB clipping threshold. Circle stems are the original signals viewed at TX and triangle stems are the distorted signals viewed at RX.

layer, like those shown in Fig. 2 ③F using the diagonal and vertical patterns.

④ Next, all non-negative layer signals are superimposed on each other to form the signal x_L, with L being the total number of layers utilised. In the FD, the original information symbols and the distortions located at the same subcarrier index are also superimposed on each other. In this way, the distortions generated by one layer will contaminate the symbols on higher layers, while layer 1 always remains free from this contamination, as shown in Fig. 2 ④F.

⑤ However, the IM/DD transmission process is subject to the maximum power emit of the LED and to the limited linearity range of other components. Hence x_L will be further clipped at a specific upper boundary (UB). For example, in Fig. 2 ⑤ B_u is used as the UB clipping threshold and the TD symbol at the 14th sample is clipped to B_u. In the FD, the UB clipping distortion will spread across the entire spectrum and will contaminate all subcarriers, as seen in Fig. 2 ⑦, where the dark grey bricks on the top represent the UB clipping distortion. The final signal ready for intensity modulation is denoted as $x_{\mathrm{UBc},L}$.

⑥ $x_{\mathrm{UBc},L}$ is then transmitted over the optical IM/DD channel, and received by the RX of Fig. 1 with the aid of a photo detector (PD). The received signal r_L may differ from $x_{\mathrm{UBc},L}$ due to the thermal noise introduced. However, in Fig. 2 we assumed a perfect channel free from thermal noise, thus $x_{\mathrm{UBc},3}$ and r_3 use the same plot in Fig. 2 ⑥.

⑦ The received TD signal is firstly transformed by an N-point IFFT into the FD signal R_L at the RX of Fig. 1. The symbols of all layers and their corresponding LB clipping distortions, together with the UB clipping distortion all co-exist at the moment, as shown in Fig. 2 ⑦.

⑧ At the RX of Fig. 1, the detection has to be carried out on a layer-by-layer basis, commencing from the first layer. Since the first layer has suffered from no LB distortion, the symbols located at those subcarrier positions can be directly extracted from R_L as $\hat{R}_1$ and a decision can be made to obtain the first layer's symbol stream $\hat{S}_1$, as shown in Fig. 2 ⑧1.

⑨ Then, $\hat{S}_1$ is assembled into the length-N signal $\tilde{\hat{S}}_1$ as in (1) and it is transformed by the IFFT into the corresponding TD signal $\hat{s}_1$. Due to the unavoidable UB clipping distortion encountered, $\hat{s}_1$ would be slightly different from s_1, as seen in Fig. 2 ⑨1, where the circles represent the original signal s_1, while the triangle markers represent the locally generated $\hat{s}_1$.

⑩ Then, $\hat{s}_1$ is clipped again at LB zero for forming the non-negative signal $\lfloor \hat{s}_1 \rfloor$.

⑪ The LB distortion of the first layer may now be generated at the RX of Fig. 1 as $\hat{I}_1$ by applying the N-point FFT to $\lfloor \hat{s}_1 \rfloor$. Again, owing to the UB clipping distortion, the LB distortion $\hat{I}_1$ generated locally at the RX of Fig. 1 will be slightly different from the actual distortion I_1, as shown in Fig. 2 ⑪1, where the small light grey bricks at the top of the LB distortion bricks constituted by the even-index bars marked by the North East hatching pattern represent this difference.

⑧ ($l = 2$) At this stage, the iterative receiver now turns to decontaminating the second layer. Hence locally generated LB distortion sample $\hat{I}_1$ of the first layer constituted by the even-index bars marked by the North East hatching pattern is subtracted from R_3 of stage ⑦, so that in the resultant $\hat{R}_2$ the symbols of the second layer can be detected without the interference from the first layer. However, the UB clipping distortion and the difference between $\hat{I}_1$ and I_1 cannot be removed, hence they slightly degrade the performance of the second layer, as shown in Fig. 2 ⑧2.

⑨ ($l = 2$) Now the second layer symbols $\hat{S}_2$ may be invoked for regenerating its LB clipping distortion for supporting the detection of the third layer, using the procedure mentioned above.

The RX of Fig. 1 keeps on activating the iteration loop ⑧∼⑪ until all layers become detected.

Moreover, assuming that the same modulation scheme is applied to all layers, we have to use a fair power allocation scheme where the power assigned is commensurate with the number of subcarriers occupied by each layer N_l. Hence the average symbol power P_l^{base} of layer l should be half that of layer $(l-1)$, yielding

$$P_l^{\mathrm{base}} = \frac{1}{2} P_{l-1}^{\mathrm{base}} = \cdots = \frac{1}{2^k} P_1^{\mathrm{base}}. \tag{2}$$

Electrical power/energy is considered here instead of the optical power/energy, as in [12].

III. BER PERFORMANCE ANALYSIS

In this section, the non-Gaussian statistical characteristics of LACO-OFDM signals will be studied, which assists us in the analysis of the BER performance.

A. PDF AND CDF OF LACO-OFDM TD SIGNALS

Some of the basics of the LACO-OFDM signal PDF were presented in [33], with the PDF for the lth base layer $\lfloor s_l \rfloor$ given as

$$g_l(z;\sigma_l) = \frac{1}{2}\delta(z) + \phi(z;\sigma_l^2)u(z), \quad z \in \mathbb{R}, \tag{3}$$

where $\delta(\cdot)$ is the Dirac delta function and $\phi(z;\sigma^2) = \frac{1}{\sqrt{2\pi}\sigma}\exp\left[-\frac{(z)^2}{2\sigma^2}\right]$ is the PDF of a zero-mean Gaussian distribution having a variance of σ^2, with $u(\cdot)$ being the Heaviside step function, while σ_l represents the root mean square (RMS) of the unclipped base layer signal s_l, while obeys $\sigma_l^2 = 2^{-l}\sigma_1^2$ according to (2) [17]. Based on (3), the PDF of an L-layer LACO-OFDM signal, denoted as $f_L(x)$, can be obtained by successively convolving (*) the PDFs of all L of its

constituent base layers, yielding [33]

$$\begin{aligned} f_L(z) &= g_1(z) * g_2(z) * \cdots * g_L(z) \\ &= \int_{z_{L-1}=-\infty}^{z_{L-1}=\infty} \int_{z_{L-2}=-\infty}^{z_{L-2}=\infty} \cdots \int_{z_1=-\infty}^{z_1=\infty} \\ &\quad \times [g_L(z - z_{L-1}) g_{L-1}(z_{L-1} - z_{L-2}) \\ &\quad \cdots g_2(z_2 - z_1) g_1(z_1)] \, \mathrm{d}z_{L-1} \mathrm{d}z_{L-2} \cdots \mathrm{d}z_1. \end{aligned} \quad (4)$$

However, due to the involvement of the term $\int \phi(z) \int \phi(z') \, \mathrm{d}z' \, \mathrm{d}z$, it has been shown in [34] that no closed form expression can be obtained for $l > 3$ layers, when (2) is applied. Therefore, we have to resort to numerical computation of the PDF solution, which is extremely time-consuming. Fortunately, the complexity of this calculation can be slightly reduced by combining pairs of convolutions, yielding

$$f_L(z) = [g_1(z) * g_2(z)] * [g_3(z) * g_4(z)] * \ldots \quad (5)$$

since the double-layer PDFs of $f_1(z)$ and $f_2(z)$ have been derived in closed-forms in [33].

When UB clipping is applied to the combined signal x_L with the clipping voltage set to B_u Volts ($B_u > 0$), the PDF of $x_L < B_u$ remains the same, while the $x_L \geq B_u$ part is truncated and replaced with a pulse $\delta(x_L - B_u)\mathcal{D}_L$, where $\mathcal{D}_L$ is given by

$$\mathcal{D}_L = \int_{B_u}^{+\infty} f_L(x_L) \, \mathrm{d}x_L = 1 - \int_0^{B_u} f_L(x_L) \, \mathrm{d}x_L. \quad (6)$$

This leads to the following expression for the PDF of the final transmitted signal $x_{\mathrm{UBc},L}$

$$f_{\mathrm{UBc},L}(x_L) = f_L(x_L) u(-x_L + B_u) + \delta(x_L - B_u)\mathcal{D}_L. \quad (7)$$

Finally, the cumulative distribution function (CDF) of signal x_L can be expressed as

$$F_L(x_L) = \int_{-\infty}^{x_L} f_L(z) \, \mathrm{d}z = \int_{0^-}^{x_L} f_L(z) \, \mathrm{d}z, \quad (8)$$

while for $x_{\mathrm{UBc},L}$ its CDF would have $f_L(\cdot)$ substituted by $f_{\mathrm{UBc},L}(\cdot)$.

B. BER PERFORMANCE EXPRESSIONS

In the IM/DD LACO-OFDM scheme, four major differences appear compared to conventional RF communications.

- Despite the fact that the signal suffers from complex-valued noise during communication, the optical signal modulated according to IM/DD scheme only deals with the real parts. Therefore the imaginary part of the TD noise does not affect the communications quality, which halves the degradation by AWGN.
- The diodes at the TX have limited dynamic ranges, thus they might require clipping of the signal amplitude at the UB. Due to the complicated non-Gaussian PDF of the LACO-OFDM signal, the clipping effects require particular attention.
- For LACO-OFDM, the decision errors of a specific layer degrade the following layers. Furthermore, the RX also imposes clipping distortion.
- Due to the multi-layer nature of LACO-OFDM, both the number of layers and the modulation scheme utilised on each layer would affect the overall bit rate, which in turn affects the energy per bit, E_b.

The following parts of this subsection discuss the influence of the last three points on the BER.

1) CLIPPING

According to Sec. II, LACO-OFDM experiences both at LB and UB clipping. Their effects will be discussed separately. For each of the base layer signals that are clipped at the LB ($s_l \rightarrow \lfloor s_l \rfloor$), the power is halved, but no information loss is observed due to the the symmetric nature of ACO-OFDM. The clipping distorts the signal and reduces its power, which may be amplified to naturally compensate for the clipping induced power-reduction. However, the UB clipping of the combined signal x_L has a more severe effect. Specifically, the UB clipping reduces the signal energy of x_L, which again may be modelled by a simple attenuation factor κ that is related to the clipping threshold B_u (corresponding to a clipping ratio of $\tau = 20\log_{10}(B_u/\sqrt{P_L})$, where P_L is the power of x_L to be given in (26)). This UB clipping can be compensated in the same way as for LB clipping, while the estimation of the value κ can be performed at the RX with the aid of a training sequence. On the other hand, the non-linear process also introduces upper harmonics that may spread across all subcarriers. A simplified model of clipping distortion based on [35] is given below, where the power of the clipped part quantifies the clipping distortion of

$$\sigma_c^2 = \int_{B_u}^{+\infty} (x_L - B_u)^2 f_L(x_L) \, \mathrm{d}x_L. \quad (9)$$

Therefore, the clipping process affects the equivalent communication signal-to-noise ratio (SNR) by reducing the power of the signal and by increasing the noise power, which undoubtedly degrades the BER performance.

2) INTER-LAYER INTERFERENCE

Each base layer of LACO-OFDM generates its own inter-layer interference and influences that of its higher layers.

At the RX, the first layer's signal (represented as $\hat{S}_1$ in FD) is immune to this and can be detected directly. According to [29], the lth layer ($l > 1$) of the LACO-OFDM signal can be detected at the RX according to

$$\hat{S}_l[k] = \arg\min_{X \in \mathcal{S}} \left| H[2^{l-1}k]X - 2\hat{R}_l[k] \right|, \quad k = 1, 3, \ldots, N/2^{l-1} - 1 \quad (10)$$

where $\hat{S}_l$ of length $N/2^{l-1}$ represents the detected signal, H is the channel state information and $\hat{R}_l$ is the lth base layer signal obtained at the RX by subtracting all the distortions generated by the former layers from the originally received FD signal R_L, yielding

$$\hat{R}_l[k] = R_L[2^{l-1}k] - H[2^{l-1}k] \sum_{i=1}^{l-1} \hat{I}_i[2^{l-i}k]. \quad (11)$$

Here, $\hat{I}_i$ represents the clipping distortion created by layer i at the receiver, which is generated by

$$\hat{I}_i = \mathcal{F}\left(\lfloor \hat{s}_i \rfloor\right) = \mathcal{F}\left(\left\lfloor \mathcal{F}^{-1}\left(\hat{\tilde{S}}_i\right)\right\rfloor\right), \tag{12}$$

where $\mathcal{F}$ and $\mathcal{F}^{-1}$ denote the Fourier transform and inverse Fourier transform, respectively.

Therefore, if an error is made when making a decision for layer l, so that $\hat{S}_l[k] \neq S_l[k]$, not only will it affect the BER behaviour of the current layer, but it will also spread across all its following layers (layers $l+1 \sim L$). More specifically, as we have assumed previously, only single symbol detection errors are considered, which is equivalent a Hamming distance of 1. In this way, the interference generated by a single decision error can be quantified as the nearest constellation pattern distance $d_{\min}$ from the symbol set $\mathcal{S}$. After the re-generation process including the IFFT, asymmetric clipping and FFT, this error propagation process will contaminate all the $N/2^{l-1}$ subcarriers, just like its clipping noise does. Hence, when considering the BER of a specific layer, in addition to the AWGN noise inflicted by the channel, the interference imposed by all its previous layers should also be taken into account. The inter-layer interference $\mathcal{G}_i$ generated by the ith layer can be calculated from the symbol error ratio (SER) $\mathbb{P}_{s,i}$ of the ith layer (to be derived later) and its corresponding quantified interference $d_{\min}$ for each single symbol error, yielding

$$\mathcal{G}_i = \mathbb{P}_{s,i} \cdot d_{\min}^2. \tag{13}$$

Thus, the cumulative sum of all its previous layers' interferences, namely $\sum_{i=1}^{l-1} \mathcal{G}_i$, should be included when calculating the energy-per-bit-to-noise-power-spectral-density ratio $\gamma_{b,l}$ of the lth layer.

3) LACO-OFDM BIT RATE

Assuming that the lth layer uses the constellation size of M_l, the corresponding number of information bits transmitted by this layer becomes:

$$\mathcal{I}_l = \frac{N}{2^{l+1}} \log_2 M_l. \tag{14}$$

Then the total amount of information transmitted by an L-layer LACO-OFDM signal would be

$$\mathcal{I}'_L = \sum_{l=1}^{L} \mathcal{I}_l = N \cdot \sum_{l=1}^{L} 2^{-l-1} \log_2 M_l. \tag{15}$$

Hence, for LACO-OFDM, the overall energy-per-bit-to-noise-power-spectral-density ratio γ_b and the symbol-energy-to-noise ratio E_s/N_0 have the following relationship

$$\frac{E_s}{N_0} = \gamma_b \cdot \sum_{l=1}^{L} 2^{-l-1} \log_2 M_l. \tag{16}$$

4) OVERALL BER PERFORMANCE

The BER and SER performance under an AWGN channel for the lth layer of the LACO-OFDM, which relies on an M_l-QAM modulation scheme, will be dependent both on the clipping distortion as well as on the BER performance of all its previous layers, which can be expressed as [13]

$$\mathbb{P}_{e,l} \approx \frac{2(\sqrt{M_l}-1)}{\sqrt{M_l} \cdot \log_2 \sqrt{M_l}} \cdot Q\left(\sqrt{\frac{3\Gamma_{s,l} \log_2 M_l}{M_l - 1}}\right), \tag{17}$$

$$\mathbb{P}_{s,l} \approx \frac{\sqrt{M_l}-1}{\sqrt{M_l}} \cdot 4 \cdot Q\left(\sqrt{\frac{3\Gamma_{s,l} \log_2 M_l}{M-1}}\right), \tag{18}$$

where $Q(\cdot)$ is the tail probability of the standard normal distribution and $\Gamma_{s,l}$ is the signal-to-noise-and-interference-plus-distortion ratio of the lth layer. For $l > 1$, $\Gamma_{s,l}$ can be expressed as

$$\Gamma_{s,l} = \frac{\kappa^2 E_s}{N_0 + \sum_{i=1}^{l-1} \mathcal{G}_i + \sigma_c^2} = \frac{\kappa^2 \gamma_b N_0 \sum_{l=1}^{L} (2^{-l-1} \log_2 M_l)}{N_0 + \sum_{i=1}^{l-1} \mathcal{G}_i + \sigma_c^2}. \tag{19}$$

For the first layer, the cumulative sum in the middle of the denominator can be neglected. Furthermore, if no UB clipping is considered, both κ and σ_c^2 can be omitted. Therefore, the overall BER performance of the LACO-OFDM system is given by the weighed average of each layer:

$$\mathbb{P}_e = \frac{1}{\sum_{l=1}^{L} 2^{-l} \log_2 M_l} \sum_{l=1}^{L} 2^{-l} \mathbb{P}_{e,l} \log_2 M_l. \tag{20}$$

According to (19), the clipping distortion is the major BER contributor when γ_b is high. Meanwhile, (9) shows that the clipping distortion is closely related to the upper tail of the signal's PDF, in other words to the signal's PAPR. Therefore, the next section will analyse the PAPR distribution of the LACO-OFDM signal in order to reveal the major factors influencing the clipping distortion.

IV. PAPR DISTRIBUTION ANALYSIS

In this spirit we embark on analysing the LACO-OFDM PAPR with the goal of avoiding the typically high BER performance degradation imposed by the clipping distortion. This section studies the LACO-OFDM PAPR as a function of the number of its layers and then in the next section develops a PAPR reduction method.

A. MOMENTS OF LACO-OFDM TD SIGNALS

According to (3), the mean square of the lth layer's signal is given by

$$P_l^{\text{base}} = E[\lfloor s_l \rfloor^2] = \int_{-\infty}^{+\infty} z^2 \, g_l(z;\sigma_l)\,\mathrm{d}z = \int_{-\infty}^{+\infty} \left[\frac{1}{2} z^2 \delta(z) + z^2 \phi(z;\sigma_l^2) u(z)\right] \mathrm{d}z = \frac{\sigma_l^2}{2}. \tag{21}$$

The mean and variance of s_l can then be expressed as

$$\begin{aligned} E[\lfloor s_l \rfloor] &= \int_{-\infty}^{+\infty} z g_l(z;\sigma_l)\,\mathrm{d}x \\ &= \int_{-\infty}^{+\infty} \left[\frac{1}{2}z\delta(z) + z\phi(z;\sigma_l^2)u(z)\right]\mathrm{d}z \\ &= \frac{\sigma_l}{\sqrt{2\pi}} = \frac{\sigma_1}{2^{l/2}\sqrt{\pi}}, \end{aligned} \tag{22}$$

and

$$\begin{aligned} D[\lfloor s_l \rfloor] &= E[\lfloor s_l \rfloor^2] - E^2[\lfloor s_l \rfloor] = \frac{\sigma_l^2}{2} - \left(\frac{\sigma_l}{\sqrt{2\pi}}\right)^2 \\ &= \frac{\pi-1}{2\pi}\sigma_l^2 = \frac{\pi-1}{2^l\pi}\sigma_1^2. \end{aligned} \tag{23}$$

Since the signals of different layers are independent from each other before their superposition, the co-variance between any two of them is zero. Hence the mean and variance of the combined signal $x_L = \sum_{l=1}^{L} \lfloor s_l \rfloor$ becomes:

$$\begin{aligned} E[x_L] &= \sum_{l=1}^{L} E[\lfloor s_l \rfloor] = \sum_{l=1}^{L} \frac{\sigma_l}{\sqrt{2\pi}} = \frac{\sigma_1}{\sqrt{\pi}} \sum_{l=1}^{L} \frac{1}{\sqrt{2}^l} \\ &= \frac{(1-2^{-L/2})\sigma_1}{(\sqrt{2}-1)\sqrt{\pi}}, \end{aligned} \tag{24}$$

$$\begin{aligned} D[x_L] &= \sum_{l=1}^{L} D[\lfloor s_l \rfloor] = \sum_{l=1}^{L} \frac{\pi-1}{2^l\pi}\sigma_1^2 \\ &= \frac{\sigma_1^2(\pi-1)}{\pi} \sum_{l=1}^{L} \frac{1}{2^l} = \frac{\sigma_1^2(\pi-1)}{\pi}\left(1 - \frac{1}{2^L}\right). \end{aligned} \tag{25}$$

Thus, the power of a L-layer LACO-OFDM signal can be expressed as

$$\begin{aligned} P_L &= E[x_L^2] = D[x_L] + E^2[x_L] \\ &= \frac{\sigma_1^2}{\pi}\left[\frac{\left(1-2^{-L/2}\right)^2}{3-2\sqrt{2}} + (\pi-1)\left(1-\frac{1}{2^L}\right)\right]. \end{aligned} \tag{26}$$

B. PAPR DISTRIBUTION

For a length-N LACO-OFDM signal x_L composed of L layers, the CDF of its PAPR can be formulated as

$$P(\mathrm{PAPR}_L \le z) = P\left(\frac{\max_{0\le n\le N-1} x_L^2[n]}{P_L} \le z\right), \tag{27}$$

where P_L is the average signal energy of the L-layer LACO-OFDM signal x_L expressed in (26). This can be further simplified as

$$\begin{aligned} P(\mathrm{PAPR}_L \le z) &= P\left(\max_{0\le n\le N-1} x_L[n] \le \sqrt{P_L z}\right) \\ &= P\left(x_L[n] \le \sqrt{P_L z},\ n = 0,\ldots,N-1\right). \end{aligned} \tag{28}$$

Since x_L can be expanded as the sum of its L unipolar base layer signals, for the nth symbol within the signal, we have

$$x_L[n] = \lfloor s_1[n] \rfloor + \lfloor s_2[n] \rfloor + \cdots + \lfloor s_L[n] \rfloor. \tag{29}$$

Recall that the energy of the symbols on each base layer $\lfloor s_l[n] \rfloor$ decreases exponentially as the layer index l increases. Hence the statistical characteristics of the signal x_L are dominated by the *first* layer's signal $\lfloor s_1 \rfloor$.

Due to the Hermitian symmetry and asymmetrical clipping, the relationship between the symbol pairs $\lfloor s_l[n] \rfloor$ and $\lfloor s_l[n+\frac{N}{2}] \rfloor$ (assuming $0 \le n < \frac{N}{2}$) becomes as follows. If the symbol obeys $\lfloor s_1[n] \rfloor > 0$, indicating that it was not clipped during the LB clipping process, the corresponding symbol $\lfloor s_1[n+\frac{N}{2}] \rfloor$ will then become 0, because the unclipped $s_1[n] = -s_1[n+\frac{N}{2}]$ and the symbol on the right hand side is clipped. The probability of having $\lfloor s_1[n] \rfloor > 0$ is $\frac{1}{2}$, which is a consequence of their independent distribution. Moreover, $\lfloor s_1[n] \rfloor > 0$ is independent of the rest of the symbols in the signal stream. Therefore (28) can be re-written based on [17]

$$P(\mathrm{PAPR}_L \le z) = \left\{P\left[x_L[0] \le \sqrt{P_L z}, x_L[N/2] \le \sqrt{P_L z}\right]\right\}^{\frac{N}{2}}. \tag{30}$$

The law of full probability can assist us in further simplifying (30) by considering the cases, when either $\lfloor s_1[n] \rfloor$ or $\lfloor s_1[n+\frac{N}{2}] \rfloor$ is zero, yielding:

$$\begin{aligned} &P\left[x_L[0] \le \sqrt{P_L z}, x_L[N/2] \le \sqrt{P_L z}\right] \\ &= P\left[x_L[0] \le \sqrt{P_L z}, x_L[N/2] \le \sqrt{P_L z}, \lfloor s_1[0] \rfloor > 0\right] \\ &\quad + P\left[x_L[0] \le \sqrt{P_L z}, x_L[N/2] \le \sqrt{P_L z}, \lfloor s_1[N/2] \rfloor > 0\right] \\ &= P\left[x_L[0] \le \sqrt{P_L z}, \lfloor s_1[0] \rfloor > 0\right] \\ &\quad + P\left[x_L[N/2] \le \sqrt{P_L z}, \lfloor s_1[N/2] \rfloor > 0\right] \\ &= 2P\left[x_L[0] \le \sqrt{P_L z}, \lfloor s_1[0] \rfloor > 0\right] \\ &= 2\left[F_L(\sqrt{P_L z}) - \frac{1}{2}\right], \end{aligned} \tag{31}$$

where $F_L(x_L)$ is the CDF of the signal x_L according to (8). Therefore, the CDF of the PAPR can be expressed as

$$\begin{aligned} P(\mathrm{PAPR}_L \le z) &= \left[2F_L(\sqrt{P_L z}) - 1\right]^{\frac{N}{2}} \\ &= \left[2\int_{-\infty}^{\sqrt{P_L z}} f_L(x_L)\,\mathrm{d}x_L - 1\right]^{\frac{N}{2}}. \end{aligned} \tag{32}$$

Then, the CCDF of the signal can be easily obtained as

$$P(\mathrm{PAPR}_L > z) = 1 - P(\mathrm{PAPR}_L \le z). \tag{33}$$

For LACO-OFDM consisted by more layers, less zeros would be found on the TD signal, due to the superposition of more layers. Meanwhile, the average power of the signal increases faster than the peak power as more layers are utilised. More specifically, if we were to fix the average signal power of the different layers, we would find that the CDF of the higher layer LACO-OFDM would become more steep, which is formulated as:

$$F_{L_1}(z) \ge F_{L_2}(z), \quad \text{for } L_1 > L_2 \text{ and } P_{L_1} = P_{L_2}. \tag{34}$$

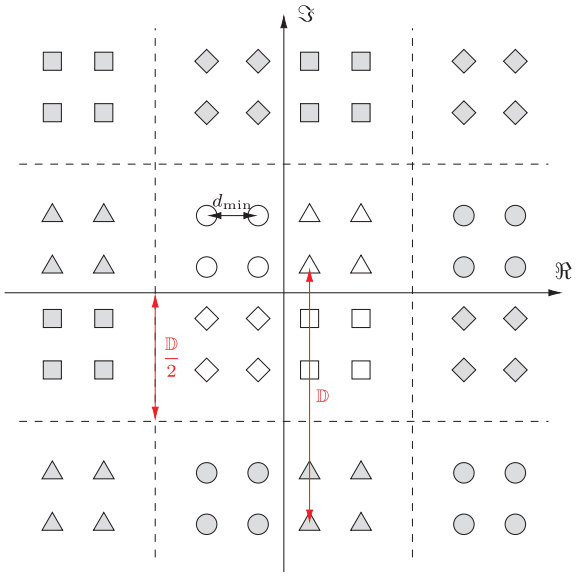

FIGURE 3. Constellation diagram of 16QAM featuring tone-injection technique. Points of same marker indicate possible shifting locations when modified.

This yields that the probability $P(\text{PAPR}_L \leq z)$ increases with L. In other words, the higher layer LACO-OFDM signals tend to have a lower PAPR than the lower layer signals. Therefore, it is plausible that LACO-OFDM mitigates the PAPR problem.

V. PERFORMANCE IMPROVEMENT

Although increasing the number of layers reduces the PAPR, further improvements may be achieved with the aid of tone injection [16], [23], as demonstrated in this section. We continue with the signal model of the proposed method, followed by the conversion of the PAPR reduction problem into a mixed integer linear programming (MILP) problem. A further simplification of the optimisation problem using l_1-minimisation is also proposed.

A. LACO-OFDM SIGNALS RELYING ON TONE-INJECTION

For each of the symbols in the original FD signals S_l, an additional symbol is added to it, i.e.

$$Y_l[k] = S_l[k] + T_l[k], \quad l = 1, 2, \ldots, L, \quad k = 0, 1, \ldots, N_l/4 - 1 \tag{35}$$

where T_l is the injected signal and Y_l is the resultant signal. The modified symbol will shift the corresponding point in the constellation diagram to one of a few legitimate locations and can be recovered losslessly at the RX by the modulo operation, regardless of which location it was shifted to.

Figure 3 shows an example of the constellation pattern of a 16QAM signal, demonstrating the tone-injection method. The 16 white markers in the centre are the constellation patterns of the original signal S_l. The real and imaginary parts of the symbol may or may not be shifted by a constant distance $\mathbb{D}$ for mitigating the PAPR. When shifting by $\mathbb{D}$ is invoked, this may shift the related constellation point to other quadrants. The full set of markers shown in Fig. 3 represents the legitimate constellation points in Y_l, while the shaded ones represent the shifted points, whose original markers are of the same shape but filled with white colour and located in the centre. Clearly, a decision threshold of $\frac{\mathbb{D}}{2}$ can be set for both the real and imaginary branches in order to classify the points into two categories, namely those that are shifted and those that remain in their original place. Based on the quadrant symmetry observed in Fig. 3, the RX eliminates the shifting of the points by invoking the modulo-$\frac{\mathbb{D}}{2}$ operation to find the corresponding original position, hence recovering the signal losslessly.

The signal T_l is appropriately selected so that the resultant signal Y_l exhibits a reduced PAPR, where each subcarrier symbol of it can be decomposed as

$$T_l[k] = -\text{sgn}(\Re\{S_l[k]\})p_l[k]\mathbb{D} - j\text{sgn}(\Im\{S_l[k]\})q_l[k]\mathbb{D}, \tag{36}$$

where $\text{sgn}(\Re\{\cdot\})$ and $\text{sgn}(\Im\{\cdot\})$ return the sign of the real and imaginary parts of the symbol, so that only un-shifted symbols will stay within the original quadrant. p and q are Booleans used to indicate whether or not the real and imaginary parts will be shifted, respectively, where 1 represents shifting and 0 the absence of it, formulated as

$$p_l[k] \in \{0, 1\}, \quad q_l[k] \in \{0, 1\}, \quad l = 1, 2, \ldots, L, \quad k = 0, 1, \ldots, (N_l/4 - 1). \tag{37}$$

Still referring to (36) and Fig. 3, $\mathbb{D} = \rho d_{\min}\sqrt{M}$ quantifies the shifting, where $\rho > 1$ is a scaling factor, $d_{\min}$ is the minimum symbol distance and $d_{\min} = 2\sqrt{\frac{3}{2(M-1)}}$ for M-QAM having a unity average symbol energy, where M is the number of constellation points in the modulation scheme.

The subcarrier symbols of the resultant signals Y_l are then mapped to their desired subcarriers in the usual manner to form $\tilde{Y}_l$ in the FD as in (1), which have a length of N and satisfy the Hermitian symmetry for all layers. Then the IFFT is performed on $\tilde{Y}_l$ and the resultant TD signal of the lth layer y_l can be expressed in (38), as shown at the top of the next page. An index substitution of $m = 2^{l-1}k$ is used in the equality (a) of (38) and therefore the range of summation becomes identical for each layer.

As shown in Fig. 1, these signals will be clipped at 0 and superimposed as in

$$y'_L[n] = \sum_{l=1}^{L} \lfloor y_l[n] \rfloor, \quad n = 0, 1, \ldots, (N-1), \tag{39}$$

where $y'_L[n]$ denotes the composite L-layer LACO-OFDM signal. The PAPR of the resultant LACO-OFDM signal $y'_L[n]$ can then be expressed by substituting (39) into (27).

B. THE LINEAR OPTIMISATION PROBLEM CONSTRUCTED FOR PAPR REDUCTION

Since the signals T_l are independent from the original signals S_l for all layers, their sum will have a higher average signal

$$
\begin{aligned}
y_l[n] &= \frac{1}{\sqrt{N}}\sum_{i=0}^{N}\tilde{Y}_l[i]\mathrm{e}^{j2\pi n\frac{i}{N}} \\
&= \frac{1}{\sqrt{N}}\sum_{k=0}^{N_l/4-1}\left[(S_l[k]+T_l[k])\mathrm{e}^{j2\pi n\frac{2^lk+2^{l-1}}{N}}+(S_l^*[k]+T_l^*[k])\mathrm{e}^{j2\pi n\frac{N-(2^lk+2^{l-1})}{N}}\right] \\
&= \frac{1}{\sqrt{N}}\sum_{k=0}^{N_l/4-1}\left[S_l[k]\mathrm{e}^{j2\pi n\frac{2^lk+2^{l-1}}{N}}+S_l^*[k]\mathrm{e}^{j2\pi n\frac{N-(2^lk+2^{l-1})}{N}}\right] \\
&\quad+\frac{1}{\sqrt{N}}\sum_{k=0}^{N_l/4-1}\left\{T_l[k]\left[\cos\left(2\pi n\frac{2^lk+2^{l-1}}{N}\right)+j\sin\left(2\pi n\frac{2^lk+2^{l-1}}{N}\right)\right]\right\} \\
&\qquad+T_l^*[k]\left[\cos\left(2\pi n\frac{N-(2^lk+2^{l-1})}{N}\right)+j\sin\left(2\pi n\frac{N-(2^lk+2^{l-1})}{N}\right)\right]\Bigg\} \\
&\overset{(a)}{=}\frac{2}{\sqrt{N}}\sum_{m=0}^{N/4-1}\Re\left\{\tilde{S}_l[m]\mathrm{e}^{j2\pi n\frac{2m+2^{l-1}}{N}}\right\}+\frac{2}{\sqrt{N}}\sum_{m=0}^{N/4-1}\left\{-p_{l,m}\mathrm{sgn}(\Re\{\tilde{S}_l[m]\})\mathbb{D}\cos\left(2\pi n\frac{2m+2^{l-1}}{N}\right)\right. \\
&\qquad\left.+q_{l,m}\mathrm{sgn}(\Im\{\tilde{S}_l[m]\})\mathbb{D}\sin\left(2\pi n\frac{N-(2m+2^{l-1})}{N}\right)\right\} \qquad (38)
\end{aligned}
$$

power than either of them in isolation according to the law of energy conservation. According to (27), in order to reduce the PAPR, we have to minimise the peak power of the TD signal $y'_L[n]$.

$$\min_{p,q}\max_{0\le n\le N-1} {y'_L}^2[n], \quad \text{s.t. (37).} \qquad (40)$$

Proposition 1: The problem formulated in (40) represents minimising the maximum amplitude of the composite LACO-OFDM signal constituted by all the lower layers, which may be expressed as:

$$\min_{p,q}\max_{\substack{0\le n\le N-1\\ 1\le L'\le L}}\sum_{l=1}^{L'}y_l[n], \quad \text{s.t. (37).} \qquad (41)$$

Proof: Given that the TD signal obeys $y'_L[n]\ge 0$ and (39), the optimisation problem in (40) can be formulated as

$$\min_{p,q}\max_{0\le n\le N-1}\sum_{l=1}^{L}\lfloor y_l[n]\rfloor, \quad \text{s.t. (37).} \qquad (42)$$

Let $h_1, h_2, \ldots, h_w, \ldots$ represent the random layer indices of the LACO-OFDM signal that are not equal to each other. Since clipping guarantees that $\lfloor y_l[n]\rfloor \ge y_l[n]$, it can be deduced that at each time slot n, the composite symbol $y'_L[n]$ has a higher power than the sum of any combination of its constituent layers $y_{h_1}[n]+y_{h_2}[n]+\ldots$, i.e. we have

$$y'_L[n]\ge\sum_{w=1}^{L'}y_{h_w}[n], \quad \begin{array}{l}\forall L'\in\{1,2,\ldots,L\},\\ \forall h_w\in\{1,2,\ldots,L\},\\ \forall n\in\{0,1,\ldots,N-1\}.\end{array} \qquad (43)$$

Assuming that the sample index of the TD peak is n^*, i.e. that $\max\{y'_L[n]\}=y'_L[n^*]$, equality applies in (43) for this particular TD sample of n^*, yielding

$$y'_L[n^*]=\max_{L',h_w}\sum_{w=1}^{L'}y_{h_w}[n^*]. \qquad (44)$$

Given the specific nature of the higher layers detailed in Sec. II and the Hermitian symmetry, the TD samples of each layer have to satisfy

$$
\begin{aligned}
y_1[n] &= -y_1[n+\frac{N}{2}], \\
y_2[n] &= -y_2[n+\frac{N}{4}]=y_2[n+\frac{N}{2}]=-y_2[n+\frac{3N}{4}], \\
y_3[n] &= -y_3[n+\frac{N}{8}]=y_3[n+\frac{N}{4}]=-y_3[n+\frac{3N}{8}] \\
&= y_3[n+\frac{N}{2}]=-y_3[n+\frac{5N}{8}]=y_3[n+\frac{3N}{4}] \\
&= -y_3[n+\frac{7N}{8}], \\
&\ldots
\end{aligned} \qquad (45)
$$

Let us now assume that the maximum in (44) is found when $L'=1$. Assume furthermore that $h_1=2$ and $n^*\le\frac{N}{2}-1$, where n^* is the TD sample index of the maximum, when the symbols of all layers other than of layer 2 are clipped. Since at $n=n^*$ the first layer's symbol is clipped, $y_1[n^*]<0$, and obviously $y_1[n^*+\frac{N}{2}]=-y_1[n^*]>0$, as shown in Fig. 4. On the other hand,

$$
\begin{aligned}
y'_L[n^*+\frac{N}{2}] &= \left\lfloor y_1[n^*+\frac{N}{2}]\right\rfloor+\left\lfloor y_2[n^*+\frac{N}{2}]\right\rfloor \\
&\quad+\sum_{l=3}^{L}\left\lfloor y_l[n^*+\frac{N}{2}]\right\rfloor
\end{aligned}
$$

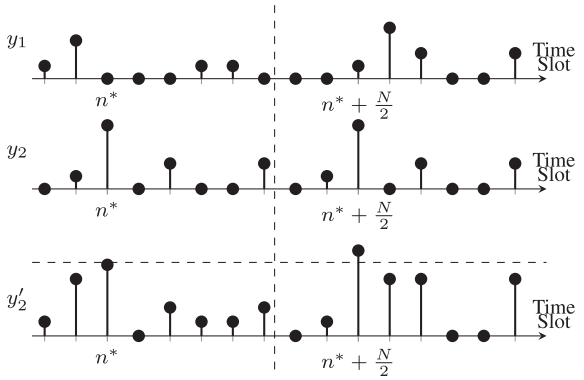

FIGURE 4. Time domain views of a 2-Layer LACO-OFDM signal, where y_1, y_2 and y_2' represent the first, second layer and the overall signal, respectively. n^* and $n^* + \frac{N}{2}$ are the time slots of interests. The vertical dashed line separates the first and second half of the time slots.

$$\begin{aligned} &= y_1[n^* + \frac{N}{2}] + y_2[n^*] \\ &> y_2[n^*] = 0 + \lfloor y_2[n^*] \rfloor + 0 \\ &= \lfloor y_1[n^*] \rfloor + \lfloor y_2[n^*] \rfloor + \sum_{l=3}^{L} \lfloor y_l[n^*] \rfloor = y_L'[n^*], \end{aligned}$$

which contradicts to the assumptions stipulated above, as shown in Fig. 4. The same conclusion can be made, when $n^* > \frac{N}{2} - 1$. Therefore, the probability of $y_L'[n^*] = y_2[n^*]$ is negligible. This process can also be further expanded to cover all situations, when $\forall L' \exists h_w$ s.t. $h_w > L' > 1$. The only legitimate combinations of the different layer-symbols left would be

$$y_L'[n^*] = \max_{L'} \sum_{l=1}^{L'} y_l[n^*]. \tag{46}$$

By substituting (46) back into (42), the equivalent problem (41) is obtained, which concludes the proof. ■

Let us now return to our PAPR optimisation problem. Let t be the target of the optimisation. Then a linear programme prototype can be formed as

$$\begin{aligned} &\min_{p,q} \ t \\ &\text{s.t.} \sum_{l=1}^{L'} y_l[n] \le t, \quad \forall 0 \le n \le N-1, \ \forall 1 \le L' \le L \\ &\quad \text{and (37).} \end{aligned} \tag{47}$$

With the aid of (38), the term $\sum_{l=1}^{L'} y_l[n]$ can be expressed in a linear form by introducing the following vectorial and matrix constants. Since (38) considers the possibility of all (n, L') combinations, the final linear form has to contain a total of (NL) rows, where each row represents the sum of the first L' layers' nth TD sample from $y_l[n]$. The first term in (38) represents the participation of the original signal S_l in Y_l, and it is identical to $s_l[n]$. A vector of length (NL) can then be formed, with the $((L'-1)N+1)$th row to the $(L'N)$th row representing the length-N summation of the first L' layers, expressed as

$$\begin{aligned} \mathbf{s} = \Bigg[& s_1[0], s_1[1], \ldots, s_1[N-1], \\ & \sum_{l=1}^{2} s_l[0], \sum_{l=1}^{2} s_l[1], \ldots, \sum_{l=1}^{2} s_l[N-1], \\ & \ldots, \sum_{l=1}^{L} s_l[N-1] \Bigg]^{\mathrm{T}}. \end{aligned} \tag{48}$$

For the second summation term in equality (a) of (38), the two parts within it can be expressed separately. For the nth time slot sample of the lth layer's TD signal, the contribution of the mth subcarrier in the corresponding FD signal T_l would be

$$c_{l,n,k} = \frac{2}{\sqrt{N}} \mathrm{sgn}(\Re\{\tilde{S}_l[k]\}) \mathbb{D} \cos\left(2\pi n \frac{2k + 2^{l-1}}{N}\right), \tag{49}$$

$$u_{l,n,k} = \frac{2}{\sqrt{N}} \mathrm{sgn}(\Im\{\tilde{S}_l[k]\}) \mathbb{D} \sin\left(2\pi n \frac{2k + 2^{l-1}}{N}\right), \tag{50}$$

where $[\cdot]^{\mathrm{T}}$ represents the transpose of a vector or matrix. The terms corresponding to different time slot samples can be grouped into vectors, and the vectors corresponding to different FD symbols of the same layer can be further grouped into vectors, yielding

$$\mathbf{c}_{l,n} = \left[c_{l,n,0}, c_{l,n,1}, \ldots, c_{l,n,N/4-1}\right]^{\mathrm{T}}, \tag{51}$$

$$\mathbf{C}_l = \left[\mathbf{c}_{l,0}, \mathbf{c}_{l,1}, \ldots, \mathbf{c}_{l,N-1}\right]^{\mathrm{T}}, \tag{52}$$

$$\mathbf{u}_{l,n} = \left[u_{l,n,0}, u_{l,n,1}, \ldots, u_{l,n,N/4-1}\right]^{\mathrm{T}}, \tag{53}$$

$$\mathbf{U}_l = \left[\mathbf{u}_{l,0}, \mathbf{u}_{l,1}, \ldots, \mathbf{u}_{l,N-1}\right]^{\mathrm{T}}. \tag{54}$$

In this way, a large matrix can be constructed with the lth block row (multiple rows from the same smaller matrix) being used to calculate the summation within (47) when $L' = l$.

$$\mathbf{A} = \begin{bmatrix} -\mathbf{C}_1 & \mathbf{U}_1 & & & & & \\ -\mathbf{C}_1 & \mathbf{U}_1 & -\mathbf{C}_2 & \mathbf{U}_2 & & & \\ \vdots & \vdots & \vdots & \vdots & \ddots & & \\ -\mathbf{C}_1 & \mathbf{U}_1 & -\mathbf{C}_2 & \mathbf{U}_2 & \cdots & -\mathbf{C}_L & \mathbf{U}_L \end{bmatrix}. \tag{55}$$

Likewise, the parameters p and q can also be grouped as vectors, yielding

$$\mathbf{p}_l = [p_l[0], p_l[1], \ldots, p_l[N/4-1]]^{\mathrm{T}}, \tag{56}$$

$$\mathbf{q}_l = [q_l[0], q_l[1], \ldots, q_l[N/4-1]]^{\mathrm{T}}, \tag{57}$$

$$\mathbf{v} = \left[\mathbf{p}_1^{\mathrm{T}}, \mathbf{q}_1^{\mathrm{T}}, \mathbf{p}_2^{\mathrm{T}}, \mathbf{q}_2^{\mathrm{T}}, \ldots, \mathbf{p}_L^{\mathrm{T}}, \mathbf{q}_L^{\mathrm{T}}\right]^{\mathrm{T}}. \tag{58}$$

Concerning the vectors $\{\mathbf{p}_l[m]\}_{m=1}^{N/4-1}$, $\{\mathbf{q}_l[m]\}_{m=1}^{N/4-1}$ defined above, note that for all $m \neq 2^{l-1}k$, the corresponding vector elements should always be zero, because no symbols are mapped to those subcarriers of the corresponding layer.

In this way, the original PAPR reduction problem of (40) can be rewritten as

$$\begin{aligned} &\min_{\mathbf{v}} \ t \\ &\text{s.t. } \mathbf{s} + \mathbf{A}\mathbf{v} \leq t \cdot \mathbf{1}_{(NL\times 1)} \\ &\quad p_l[m], q_l[m] \begin{cases} \in \{0, 1\}, & m = 2^{l-1}k, \\ = 0, & \text{otherwise}, \end{cases} \end{aligned} \tag{59}$$

which is now transformed into a mixed integer linear programming (MILP) problem. Hence, off-the-shelf solvers can be applied [36].

C. SIMPLIFYING THE OPTIMISATION

It has been shown in [16] and [37] that the majority of the elements in the optimisation variable vector $\mathbf{v}$ would be zeros, indicating that with a few subcarrier symbol shifts, the PAPR may be considerably reduced. This result also shows that the vector $\mathbf{v}$ is sparse. Hence, based on [16], [23], and [38] we can further simplify the optimisation problem by minimising the l_1-norm $\|\mathbf{v}\|_1$ of the desired sparse vector $\mathbf{v}$ as

$$\begin{aligned} &\min_{\mathbf{v}} \ \|\mathbf{v}\|_1 \\ &\text{s.t. } \mathbf{s} + \mathbf{A}\mathbf{v} \leq t' \cdot \mathbf{1}_{(NL\times 1)}, \\ &\quad \mathbf{0}_{(NL/2\times 1)} \leq \mathbf{v} \leq \mathbf{1}_{(NL/2\times 1)}, \\ &\quad \mathbf{W}\mathbf{v} = \mathbf{0}_{(NL/2\times 1)}, \end{aligned} \tag{60}$$

where $\mathbf{W}$ is a diagonal matrix, whose $2^{l-1}k$th elements in the diagonal would be 1 and the rest be 0, which ensures the unused subcarriers remain unshifted. Furthermore, t' is a pre-determined peak amplitude reduction target that varies both with the number of layers L and with the number of FFT points N according to [16] and [23]. In this paper, an empirical value of $t' = 0.7$ is used for 4LACO-OFDM. It is worth mentioning that (60) relaxes the restriction formulated in (37). Thus the resultant vector $\mathbf{v}^*$ contains floating-point numbers within [0, 1]. Then, according to [16], a total of Z candidate vectors containing only 0 and 1 will be generated, each of which has a probability of being 1 given by the corresponding value in $\mathbf{v}^*$. Their PAPRs of each candidate signal are then calculated by applying (35) and the one achieving minimum PAPR would be selected as the final solution.

Again, the method proposed reduces the PAPR, which is achieved by increasing the average symbol energy, while simultaneously reducing the peak symbol energy. The peak symbol energy reduction results in beneficial UB clipping distortion reduction. As a benefit, the PAPR reduction relaxes the linearity requirement of the amplifiers and quantisers, while improving the BER performance by reducing clipping distortion. Hence a lower power is required for achieving the same BER target, which ultimately improves the energy efficiency.

VI. SIMULATION RESULTS AND DISCUSSIONS

In this section, our BER and PAPR expressions derived are verified by Monte-Carlo simulations, which are followed by further discussions. All the simulations in this section rely on the power allocation strategy of Sec. II, with the overall signal power transmitted set to $P_L = 1$ W. Table 1 summaries the parameters to be used in the following simulation results, if not been stated otherwise.

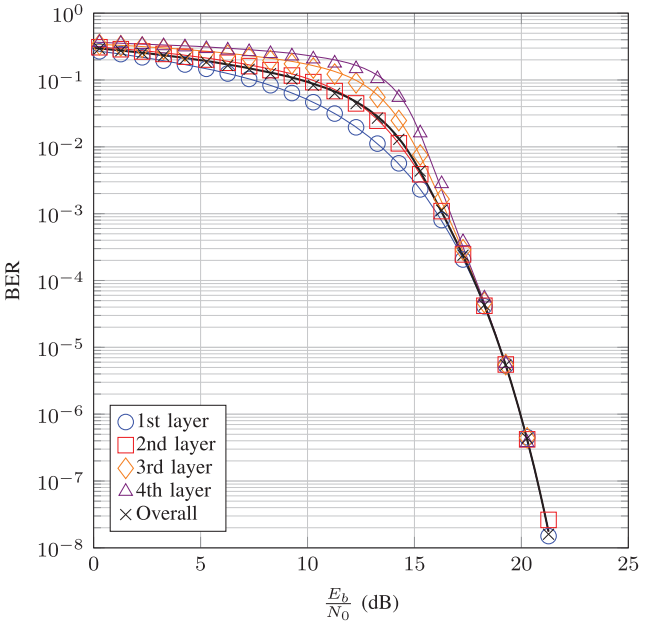

FIGURE 5. BER of all layers of 4LACO-OFDM signals for 16QAM modulation. Lines represent the theoretical values of (17), (20) and markers the simulation results. All parameters are summarised in Table 1.

Figure 5 shows the BER versus E_b/N_0 (γ_b) performance of each layer in a 4-layer LACO-OFDM (4LACO-OFDM) system without any UB clipping. The simulated BER results of the four layers are represented by the markers, while their analytical curves are marked by solid lines in all figures. The overall average BER performance of all four layers is also provided. According to Fig. 5, the four layers exhibit different BER behaviours at low SNRs. Naturally, the first layer has the best BER since no interference is imposed by the higher layers. By contrast, observed from (19) that all higher layers suffer from the inter-layer interference inflicted by the previous layers. As the SNR increases, the four BER curves tend to converge to the 16QAM BER curve. More explicitly, (13) and (17) show that as the SNR increases, the SER of the lower layers is reduced, hence the interference imposed to the higher layers is also reduced, which in turn decreases the SER of the higher layers. Gradually all the interferences turned to zero and in this way all layers start to behave the same way as the first layers, since no more inter-layer interference exists.

Figure 6 shows the BER of LACO-OFDM both with and without a $\tau = 9$ dB UB clipping operation. The derivation of (19), (20) is verified here by the simulations. As expected, the lower-throughput LACO-OFDM composed of less layers exhibit a better BER performance. On the other hand, since the PAPR of more layers is lower, they have better immunity against distortion, when clipped at the UB. Therefore, the BER curves of unclipped and clipped situations are closer

TABLE 1. Parameters used for simulation results.

Parameter	Definitions	Value	Applicable Figures
M	Size of the constellation patten	16	5, 6, 7, 8, 9, 10
L	Number of layers composing the LACO-OFDM signal	3	10
		4	5, 8
N	Number of FFT/IFFT points for scenarios without UB clipping[a]	1024	5, 6, 7, 10
		64	8, 9
τ	UB clipping ratio	9 dB	6
Z	Number of candidate vectors for PAPR reduction optimisation.	200	9, 10
N/A	Channel	AWGN	5, 6, 7, 8, 9, 10

[a]For scenarios with UB clippings, longer FFT length is required.

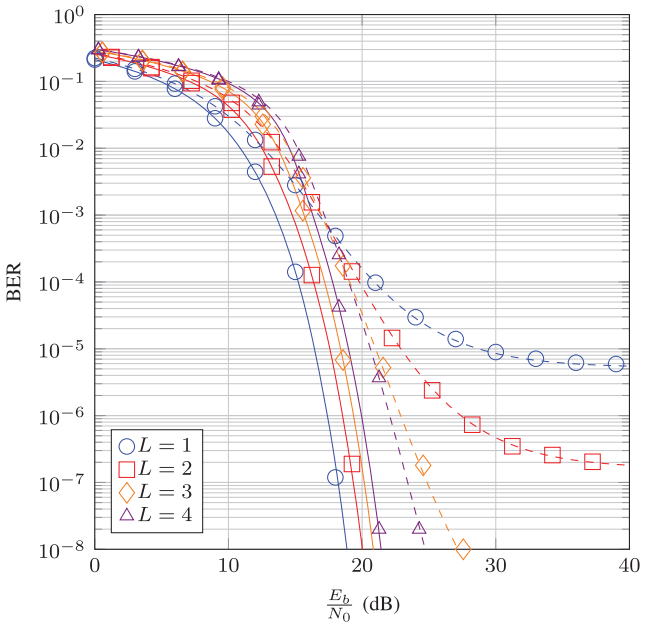

FIGURE 6. BER of all layers of 4LACO-OFDM signals for 16QAM modulation. Lines represent the theoretical values of (17), (20) and markers the simulation results. Dashed lines represent simulations with UB clipping considered, while solid lines the absence of it. All parameters are summarised in Table 1.

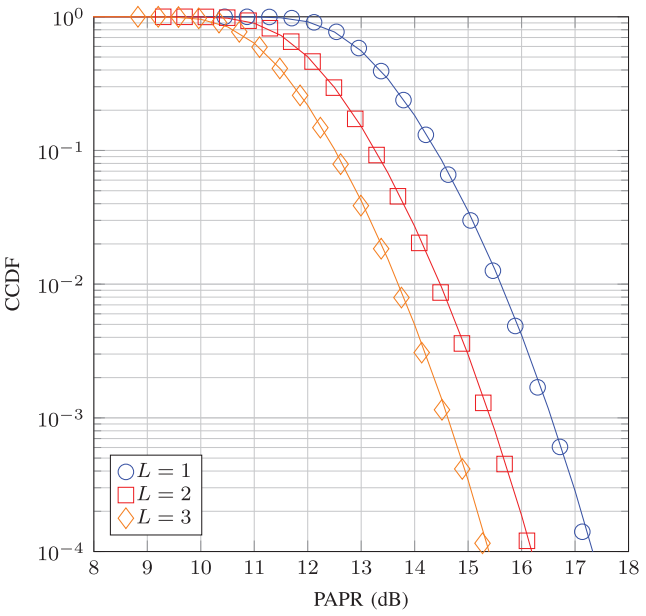

FIGURE 7. CCDF of the PAPR of 1024-subcarrier LACO-OFDM TD signals. Lines represent the theoretical values of (32) and markers the simulation results. All parameters are summarised in Table 1.

to each other for signals composed of more layers. Furthermore, the BER curves of clipped signals tend to converge at a certain level, when the UB clipping distortion dominates the performance. Thanks to their lower PAPR, the schemes having more layers suffer from less distortion at the same clipping ratio, which leads to their lower BER.

Figure 7 compares the CCDF of several LACO-OFDM time-domain signals having 1024 subcarriers. Various number of layers L are used. The trend that LACO-OFDM signal having more layers tends to exhibit lower PAPR can be clearly observed when the total number of subcarriers is fixed. This means that the peak power increases slower than the average power upon combining more layers. This is consistent with the analysis in Sec. IV-B.

Figure 8 portrays the CCDF of the proposed PAPR reduction method for 3LACO-OFDM 16QAM signals for a total of 64 subcarriers. The number of candidate solution vectors generated Z is treated as a variable and its PAPR improvement is quantified. At the CCDF $= 10^{-3}$ level, our tone-injection technique provides a PAPR reduction of around 5 dB, provided that sufficient candidate vectors are generated. Naturally, a higher PAPR improvement can be observed, when a larger Z is used, albeit at a higher computational complexity. Therefore, we struck a compromise at $Z = 200$ for our further simulation.

On the other hand, the PAPR improvement is a function of the number of layers L. Fig. 9 characterises this feature by comparing the PAPR improvement of different LACO-OFDM signals. The improvement of the PAPR at the CCDF $= 10^{-3}$ level is used for our evaluation. It is clear that the PAPR improvement is reduced as the number of layers increases. A plausible reason for this trend based on Fig. 7 is that the PAPR decreases as L increases, which in turn makes further improvements even harder to achieve. However, if we

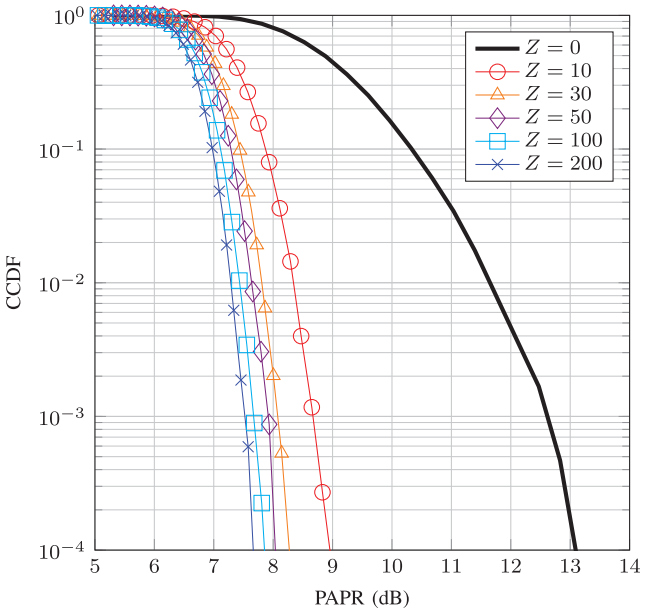

FIGURE 8. CCDF of the PAPR of LACO-OFDM TD signals from our PAPR reduction technique with different number of candidate vectors generated Z. All parameters are summarised in Table 1.

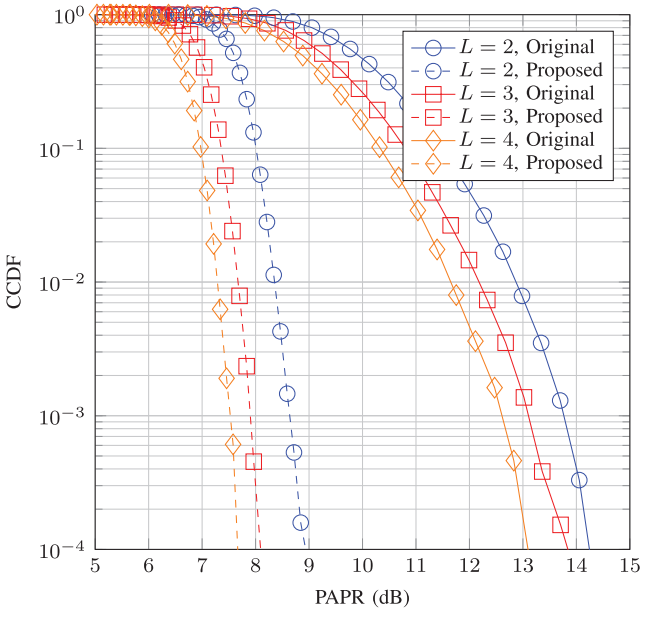

FIGURE 9. CCDF of the PAPR of LACO-OFDM TD signals. Solid lines represent the resultant signal from our PAPR reduction technique and dashed lines their original counterparts. All parameters are summarised in Table 1.

compare the PAPR of the injection-aided 4LACO-OFDM signal to the original 2LACO-OFDM, the improvement now appears more dramatic.

The influence of the proposed PAPR reduction method on the BER performance is characterised in Fig. 10. The BER versus E_b/N_0 performance of the 3LACO-OFDM signals under various clipping ratios featuring the proposed PAPR reduction method are depicted by the solid lines, together with their original direct-clipping based counterparts represented by the dashed lines. The proposed method expands the

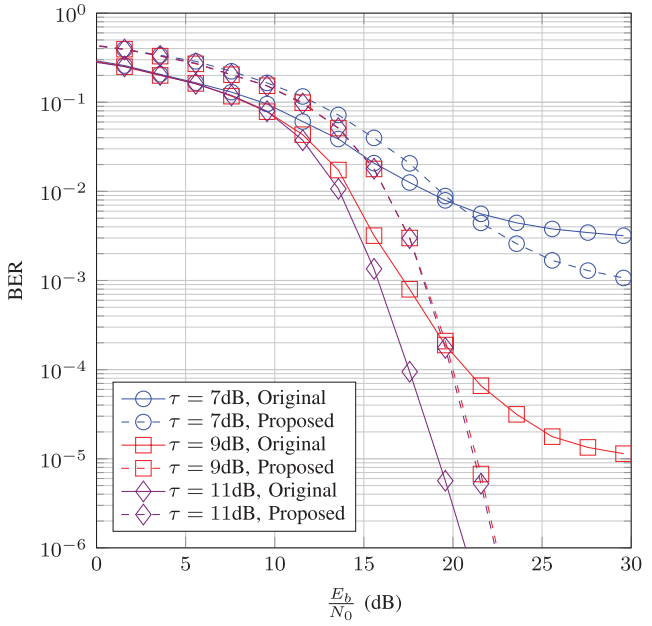

FIGURE 10. Comparison of BER performance over AWGN channel for 16QAM 3LACO-OFDM signals under different UB clipping ratios (τ). Shown in solid lines are signals gone through the proposed PAPR reduction method, while those in dashes lines are the signals without PAPR reduction.

size of the constellation pattern by shifting the constellation points to locations farther apart, while keeping the minimum distance between each pair of points the same. In this way the effective E_b/N_0 for the resultant signals becomes lower than that of their original signals, which imposes a higher information loss. However, for $\gamma_b > 20$ dB the proposed PAPR reduction technique starts to outperform its direct-clipping counterparts for both 7 dB and 9 dB clipping ratios. This is an explicit benefit of its reduced clipping distortion.

VII. CONCLUSIONS

The state-of-the-art of the LACO-OFDM scheme designed for IM/DD communications has been reviewed and new theoretical expressions of its BER and of its PAPR have been derived and verified by simulations. Explicitly, the BER performance has been analysed in the face of noise, inter-layer interference and clipping distortion. The higher layers tend to have worse BER performance due to the interference imposed by the lower layers, while the first layer has the same performance as ACO-OFDM. We demonstrated that the LACO-OFDM PAPR is significantly influenced by that of its first layer. The PAPR expression indicates that adding more layers will result in a TD signal with lower PAPR, hence LACO-OFDM attains PAPR reduction. A novel PAPR reduction method based on tone-injection was also proposed for LACO-OFDM, which is capable of achieving in excess of 5 dB PAPR reduction on top of LACO-OFDM's own reduction capability. The BER simulations also match with our analysis, demonstrating that the signals composed of more layers exhibit a better resistance against clipping, albeit their BER performance becomes much worse when, no clip-

ping is imposed. The proposed PAPR reduction method also helps improve the BER. As a result, our LACO-OFDM solution exhibits excellent spectral and energy efficiency.

ACKNOWLEDGMENT

The authors acknowledge the use of the IRIDIS High Performance Computing Facility, and associated support services at the University of Southampton, in the completion of this work. The data from the paper can be obtained from the University of Southampton institutional repository: 10.5258/SOTON/D0228.

REFERENCES

[1] R. Zhang, J. Wang, Z. Wang, Z. Xu, C. Zhao, and L. Hanzo, "Visible light communications in heterogeneous networks: Paving the way for user-centric design," *IEEE Wireless Commun.*, vol. 22, no. 2, pp. 8–16, Apr. 2015.

[2] L. Hanzo, H. Haas, S. Imre, D. O'Brien, M. Rupp, and L. Gyongyosi, "Wireless myths, realities, and futures: From 3G/4G to optical and quantum wireless," *Proc. IEEE*, vol. 100, no. Centennial Special Issue, pp. 1853–1888, May 2012.

[3] J. M. Kahn and J. R. Barry, "Wireless infrared communications," *Proc. IEEE*, vol. 85, no. 2, pp. 198–265, Feb. 1997.

[4] J. Armstrong, "OFDM for optical communications," *J. Lightw. Technol.*, vol. 27, no. 3, pp. 189–204, Feb. 1, 2009.

[5] J. B. Carruthers and J. M. Kahn, "Multiple-subcarrier modulation for nondirected wireless infrared communication," *IEEE J. Sel. Areas Commun.*, vol. 14, no. 3, pp. 538–546, Apr. 1996.

[6] J. Armstrong and B. Schmidt, "Comparison of asymmetrically clipped optical OFDM and DC-biased optical OFDM in AWGN," *IEEE Commun. Lett.*, vol. 12, no. 5, pp. 343–345, May 2008.

[7] J. Armstrong and A. J. Lowery, "Power efficient optical OFDM," *Electron. Lett.*, vol. 42, no. 6, pp. 370–372, Mar. 2006.

[8] S. C. J. Lee, S. Randel, F. Breyer, and A. M. J. Koonen, "PAM-DMT for intensity-modulated and direct-detection optical communication systems," *IEEE Photon. Technol. Lett.*, vol. 21, no. 23, pp. 1749–1751, Dec. 1, 2009.

[9] N. Fernando, Y. Hong, and E. Viterbo, "Flip-OFDM for unipolar communication systems," *IEEE Trans. Commun.*, vol. 60, no. 12, pp. 3726–3733, Dec. 2012.

[10] D. Tsonev, S. Sinanovic, and H. Haas, "Novel unipolar orthogonal frequency division multiplexing (U-OFDM) for optical wireless," in *Proc. IEEE 75th VTC*, May 2012, pp. 1–5.

[11] J. Armstrong, B. J. C. Schmidt, D. Kalra, H. A. Suraweera, and A. J. Lowery, "Performance of asymmetrically clipped optical OFDM in AWGN for an intensity modulated direct detection system," in *Proc. IEEE Global Commun. Conf.*, San Francisco, CA, USA, Nov. 2006, pp. 1–5.

[12] S. Dimitrov, S. Sinanovic, and H. Haas, "Clipping noise in OFDM-based optical wireless communication systems," *IEEE Trans. Commun.*, vol. 60, no. 4, pp. 1072–1081, Apr. 2012.

[13] A. Goldsmith, *Wireless Communications*, 1st ed. New York, NY, USA: Cambridge Univ. Press, 2005.

[14] H. Ochiai and H. Imai, "On the distribution of the peak-to-average power ratio in OFDM signals," *IEEE Trans. Commun.*, vol. 49, no. 2, pp. 282–289, Feb. 2001.

[15] S. H. Han and J. H. Lee, "An overview of peak-to-average power ratio reduction techniques for multicarrier transmission," *IEEE Wireless Commun.*, vol. 12, no. 2, pp. 56–65, Apr. 2005.

[16] N. Jacklin and Z. Ding, "A linear programming based tone injection algorithm for PAPR reduction of OFDM and linearly precoded systems," *IEEE Trans. Circuits Syst. I, Reg. Papers*, vol. 60, no. 7, pp. 1937–1945, Jul. 2013.

[17] J. Wang, Y. Xu, X. Ling, R. Zhang, Z. Ding, and C. Zhao, "PAPR analysis for OFDM visible light communication," *Opt. Exp.*, vol. 24, pp. 27457–27474, Nov. 2016.

[18] H. Chen, J. He, J. Tang, F. Li, M. Chen, and L. Chen, "Performance of 16 QAM-OFDM with new null subcarrier shifting in an intensity-modulated direct detection system," *J. Opt. Commun. Netw.*, vol. 6, no. 2, pp. 159–164, Feb. 2014.

[19] W. O. Popoola, Z. Ghassemlooy, and B. G. Stewart, "Pilot-assisted PAPR reduction technique for optical OFDM communication systems," *J. Lightw. Technol.*, vol. 32, no. 7, pp. 1374–1382, Apr. 1, 2014.

[20] J. Hou, X. Zhao, F. Gong, F. Hui, and J. Ge, "PAPR and PICR reduction of OFDM signals with clipping noise-based tone injection scheme," *IEEE Trans. Veh. Technol.*, vol. 66, no. 1, pp. 222–232, Jan. 2016.

[21] S. D. Dissanayake, K. Panta, and J. Armstrong, "A novel technique to simultaneously transmit ACO-OFDM and DCO-OFDM in IM/DD systems," in *Proc. IEEE GLOBECOM Workshops*, Dec. 2011, pp. 782–786.

[22] B. Ranjha and M. Kavehrad, "Hybrid asymmetrically clipped OFDM-based IM/DD optical wireless system," *IEEE/OSA J. Opt. Commun. Netw.*, vol. 6, no. 4, pp. 387–396, Apr. 2014.

[23] B. Li, W. Xu, H. Zhang, C. Zhao, and L. Hanzo, "PAPR reduction for hybrid ACO-OFDM aided IM/DD optical wireless vehicular communications," *IEEE Trans. Veh. Technol.*, to be published.

[24] L. Chen, B. Krongold, and J. Evans, "Successive decoding of anti-periodic OFDM signals in IM/DD optical channel," in *Proc. IEEE Int. Conf. Commun.*, Cape Town, South Africa, May 2010, pp. 1–6.

[25] H. Elgala and T. D. C. Little, "SEE-OFDM: Spectral and energy efficient OFDM for optical IM/DD systems," in *Proc. IEEE 25th Annu. Int. Symp. Pers., Indoor, Mobile Radio Commun.*, Sep. 2014, pp. 851–855.

[26] D. Tsonev, S. Videv, and H. Haas, "Unlocking spectral efficiency in intensity modulation and direct detection systems," *IEEE J. Sel. Areas Commun.*, vol. 33, no. 9, pp. 1758–1770, Sep. 2015.

[27] M. S. Islim, D. Tsonev, and H. Haas, "On the superposition modulation for OFDM-based optical wireless communication," in *Proc. IEEE Global Conf. Signal Inf. Process. (GlobalSIP)*, Dec. 2015, pp. 1022–1026.

[28] M. S. Islim and H. Haas, "Augmenting the spectral efficiency of enhanced PAM-DMT-based optical wireless communications," *Opt. Exp.*, vol. 24, pp. 11932–11949, May 2016.

[29] Q. Wang, C. Qian, X. Guo, Z. Wang, D. G. Cunningham, and I. H. White, "Layered ACO-OFDM for intensity-modulated direct-detection optical wireless transmission," *Opt. Exp.*, vol. 23, no. 9, pp. 12382–12393, May 2015.

[30] Q. Wang, Z. Wang, X. Guo, and L. Dai, "Improved receiver design for layered ACO-OFDM in optical wireless communications," *IEEE Photon. Technol. Lett.*, vol. 28, no. 3, pp. 319–322, Feb. 1, 2016.

[31] A. J. Lowery, "Comparisons of spectrally-enhanced asymmetrically-clipped optical OFDM systems," *Opt. Exp.*, vol. 24, no. 4, pp. 3950–3966, Feb. 2016.

[32] B. Song, C. Zhu, B. Corcoran, Q. Wang, L. Zhuang, and A. J. Lowery, "Experimental layered/enhanced ACO-OFDM short-haul optical fiber link," *IEEE Photon. Technol. Lett.*, vol. 28, no. 24, pp. 2815–2818, Dec. 15, 2016.

[33] Y. Sun, F. Yang, and J. Gao, "Comparison of hybrid optical modulation schemes for visible light communication," *IEEE Photon. J.*, vol. 9, no. 3, Jun. 2017, Art. no. 7904213.

[34] V. J. Francis, "On the distribution of the sum of n sample values drawn from a truncated normal population," *Suppl. J. Roy. Stat. Soc.*, vol. 8, no. 2, pp. 223–232, 1946.

[35] R. Mesleh, H. Elgala, and H. Haas, "Performance analysis of indoor OFDM optical wireless communication systems," in *Proc. IEEE Wireless Commun. Netw. Conf. (WCNC)*, Apr. 2012, pp. 1005–1010.

[36] A. Schrijver, *Theory of Linear and Integer Programming*. Chichester, U.K.: Wiley, 1998.

[37] H. Zhang, Y. Yuan, and W. Xu, "PAPR reduction for DCO-OFDM visible light communications via semidefinite relaxation," *IEEE Photon. Technol. Lett.*, vol. 26, no. 17, pp. 1718–1721, Sep. 1, 2014.

[38] D. L. Donoho, "Compressed sensing," *IEEE Trans. Inf. Theory*, vol. 52, no. 4, pp. 1289–1306, Apr. 2006.

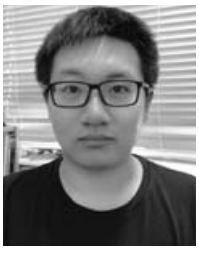

XIAOYU ZHANG (S'16) received the B.Eng. degree in electronic information engineering from the University of Electronic Science and Technology of China and the M.Sc. degree from the University of Southampton, U.K., where he is currently pursuing the Ph.D. degree with the Southampton Wireless Group. His research interests include the areas of full-duplex communications and visible light communications.

QI WANG (S'15–M'16) received the B.E. and Ph.D. degrees (Hons.) in electronic engineering from Tsinghua University, Beijing, China, in 2011 and 2016, respectively. From 2014 to 2015, he was a Visiting Scholar with the Electrical Engineering Division, Centre for Photonic Systems, Department of Engineering, University of Cambridge. Since 2016, he has been a Research Fellow with the Southampton Wireless Group, University of Southampton. He has authored over 20 IEEE/OSA journal papers and several conference papers. His research interests include modulation and signal processing for wireless communication and visible light communication. He was a recipient of the Excellent Doctoral Dissertation of Chinese Institute of Electronics, the Outstanding Ph.D. Graduate of Tsinghua University, the Excellent Doctoral Dissertation of Tsinghua University, the National Scholarship, and the Academic Star of Electronic Engineering Department, Tsinghua University. He serves as an Associate Editor of the IEEE Access and a TPC member of many IEEE conferences, including the Globecom, GlobalSIP, CSNDSP, and IWCMC.

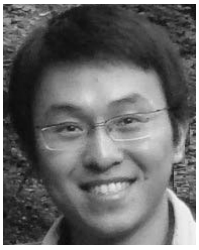

RONG ZHANG (M'09–SM'16) received the Ph.D. degree in wireless communications from the University of Southampton (UoS) in 2009. He was a Research Assistant with the Mobile Virtual Centre of Excellence, UoS, one of the U.K.'s largest industrial-academic partnerships in ICT. During his post-doctoral period in ECS, he contributed as the UoS lead researcher on a number of international projects. He took his industrial consulting leave for Huawei EU R&D as a System Algorithms Expert. He is currently an Assistant Professor with the Southampton Wireless Group, School of ECS, UoS. He has a total of over 90 IEEE/OSA publications, including over 60 journals (over 20 of which as first author). Owing to his outstanding academic achievements, he was a recipient of the prestigious Dean's Publication Award. He was also a recipient of the prestigious R.A.Eng. Industrial Fellowship. He is an R.A.Eng. Industrial Fellow, a member of the OSA, and a member of the HEA. He regularly serves as an editor/reviewer of the IEEE/OSA journals and funding bodies and has been several times as a TPC member/invited session chair of major conferences.

SHENG CHEN (M'90–SM'97–F'08) received the B.Eng. degree in control engineering from the East China Petroleum Institute, Dongying, China, in 1982, the Ph.D. degree in control engineering from City University, London, in 1986, and the D.Sc. degree from the University of Southampton, Southampton, U.K., in 2005. He held research and academic appointments with The University of Sheffield, The University of Edinburgh, and the University of Portsmouth, U.K., from 1986 to 1999. Since 1999, he has been with the Electronics and Computer Science Department, University of Southampton, where he is currently a Professor of Intelligent Systems and Signal Processing. He has authored over 550 research papers. His research interests include adaptive signal processing, wireless communications, modeling, and identification of nonlinear systems, neural network and machine learning, intelligent control system design, evolutionary computation methods, and optimization. He is a fellow of the Royal Academy of Engineering, U.K., a fellow of the IET, and a Distinguished Adjunct Professor with King Abdulaziz University, Jeddah, Saudi Arabia. He was an ISI Highly Cited Researcher in engineering in 2004.

LAJOS HANZO (M'91–SM'92–F'03) received the D.Sc. degree in electronics in 1976 and the Ph.D. degree in 1983. In 2009, he received the honorary doctorate from the Technical University of Budapest and from The University of Edinburgh in 2015. In 2016, he was admitted to the Hungarian Academy of Science. During his 40-year career in telecommunications, he has held various research and academic posts in Hungary, Germany, and the U.K. Since 1986, he has been with the School of Electronics and Computer Science, University of Southampton, U.K., where he currently holds the Chair in telecommunications. He has successfully supervised 111 Ph.D. students, co-authored 18 John Wiley/IEEE Press books on mobile radio communications totaling in excess of 10 000 pages, published 1670 research contributions at the IEEE Xplore, acted both as the TPC and the general chair of the IEEE conferences, presented keynote lectures and has been received a number of distinctions. He is currently directing a 60-strong academic research team, working on a range of research projects in the field of wireless multimedia communications sponsored by industry, the Engineering and Physical Sciences Research Council, U.K., the European Research Council's Advanced Fellow Grant, and the Royal Society's Wolfson Research Merit Award. He is an enthusiastic supporter of industrial and academic liaison and he offers a range of industrial courses. He is a fellow of the F.R.Eng., the IET, and the EURASIP. He is also a Governor of the IEEE VTS. From 2008 to 2012, he was the Editor-in-Chief of the IEEE Press and a Chaired Professor at Tsinghua University, Beijing. He has over 30 000 citations and an h-index of 68.